American Mineralogist, Volume 60, pages 359–366, 1975

Direct Observation of Metal Vacancies by High-Resolution Electron Microscopy. Part I: 4*C* Type Pyrrhotite (Fe_7S_8)

HIROMOTO NAKAZAWA[1],

National Institute for Researches in Inorganic Materials, Sakura-mura, Niihari, Ibaragi 300-31, Japan

NOBUO MORIMOTO,

Institute of Scientific and Industrial Research, Osaka University, Suita, Osaka 565, Japan

AND EIICHI WATANABE

JEOL, Ltd., 1418 Nakagami, Akishima, Tokyo 196, Japan

Abstract

The contrast in the lattice image from very thin crystals of the 4*C* type pyrrhotite (Fe_7S_8) is interpreted to be directly related to its structure through the ordered distribution of metal vacancies. Fine band structure parallel to (001) is characteristic, where the alternating bands have a thickness changing from a half to five times of the *c* length of the 4*C* type. Based on the arrangement of the vacant sites, the bands can be described to be in twin relation of 60° or 120° rotation around the c^* axis. Out-of-phase boundaries with a displacement vector of $\mathbf{c}/4$ are also observed approximately parallel to $(10\bar{2})$ or its symmetrically related planes.

Introduction

Recent development in high resolution electron microscopy permits the observation of two-dimensional lattice images that are directly correlated with the structure details (Iijima and Allpress, 1973, 1974; Allpress and Sanders, 1973). One of the important advantages of this technique compared with those of the X-ray diffraction is that the non-periodic features in crystals are imaged by the contribution from both Bragg and non-Bragg reflections.

In sulfide minerals, the ordering of metal vacancies results in many superstructures. Nonintegral superstructures in the nonstoichiometric pyrrhotites are the examples of these structures (Nakazawa and Morimoto, 1971; Morimoto, Gyobu, Tsukuma, and Koto, 1975 b). The application of the lattice image technique therefore provides information on the structure details of the nonintegral superstructures of pyrrhotites which can not be obtained by X-ray diffraction.

The application is, however, not straightforward, because the interpretation of the image contrast is difficult unless the structure is well known. Thus the lattice image technique has been applied to the stoichiometric 4*C* type pyrrhotite (Fe_7S_8) in this study because that crystal structure is well known.

On purely geometrical grounds, van Landuyt and Amelinckx (1972) predicted possible anti-phase boundaries, stacking faults, and twin boundaries associated with the ordering of vacancies in the 4*C* type pyrrhotite. They observed various boundaries in the 4*C* type by conventional electron microscopy and confirmed some of the possible interfaces.

In this investigation, the ordered arrangements of metal vacancies and the interfaces, such as twin boundaries and out-of-step boundaries in the 4*C* type pyrrhotite, have been successfully connected with the lattice image contrast obtained by a high-resolution electron microscope. A preliminary report on this work has been given by Nakazawa, Morimoto, and Watanabe (1974a) and Morimoto, Nakazawa, and Watanabe (1974).

Materials

Crystals of the 4*C* type from the Chichibu mine, Japan, were first studied by precession and powder

[1] Present address: Fachbereich Geowissenschaften: Mineralogie, Kristallographie, Petrologie, Philipps-Universität, 355 Marburg/Lahn, Deutschhausstr. 10, Germany.

methods and confirmed to be monoclinic. The cell dimensions obtained from the powder patterns are: a = 11.885(2) Å, b = 6.870(1) Å, c = 5.6990(5)×4 Å and β = 90.47(1)° (Morimoto, Gyobu, Mukaiyama, and Izawa, 1975 a).

The composition was determined to be approximately Fe_7S_8 by electron microprobe analysis using troilite (FeS) and pyrite (FeS_2) as standards. Ni, Co, and Cu were not detected (Banno and Itaya, private communication). The d value of the hexagonal *102*, determined after heating the crystals in an evacuated silica tube at 345°C for 6 minutes, is 2.0591 Å, indicating a composition of 46.80 atom percent iron, or Fe_7S_8, by Arnold's (1962) curve (Morimoto *et al,* 1975 a).

The crystals were always observed in twin relation of 60° or 120° rotation around the c^* axis no matter how small the specimens used in the precession method.

Experimental Procedure

Crystals of the 4*C* type were broken into fine fragments and mounted on microgrids using the usual procedures of sample preparation for high resolution electron microscopy (Allpress and Sanders, 1973). Lattice images were obtained at several values of underfocusing and appropriate orientations in a JEM 100B electron microscope, operated at 100 kV, with a high resolution goniometer stage. Optimum images for structural details were obtained at the range of underfocusing of approximately 1100 ± 100 Å relative to the Gaussian image plane.

Structural change and decomposition of the pyrrhotite samples were generally not observed when exposed to the electron beam. On rare occasions, the superstructure reflections gradually decreased and finally disappeared, while the main reflections remained. This indicates occasional transformation of the 4*C* type phase to the high-temperature form with the disordered NiAs-type structure. The thermal effect of the electron beam on the samples was, therefore, considered to be different from grain to grain, according to their size and thickness and their orientation relative to the perforated support film of the microgrid.

Structure of the 4*C* Type Pyrrhotite

The ordered arrangements of iron vacancies in the superstructure of the 4*C* type, based on the fundamental NiAs-type structure ($A \sim 3.45$ Å, $C \sim 5.75$ Å), was originally determined by Bertaut (1953). The structure refinement of the 4*C* type was carried out by Tokonami, Nishiguchi, and Morimoto (1971), who confirmed the result by Bertaut. In structures of the 4*C* type (Fig. 1), S atoms approximately occupy the nodes of the hexagonal closest-packing, and Fe atoms are regularly arranged in the octahedral interstices between the S atoms. The vacancies among the Fe sites are ordered and are confined to alternate layers of Fe atoms normal to the c axis. Although the vacant sites are crystallographically equivalent, they are named A, B, C, and D sites from the bottom defective layer to the top in the cell (Fig. 1). Then the structure is represented as a stacking of AFBFCFDF· · · ·, where A, B, C, and D represent the defective layers with vacant sites at A, B, C, and

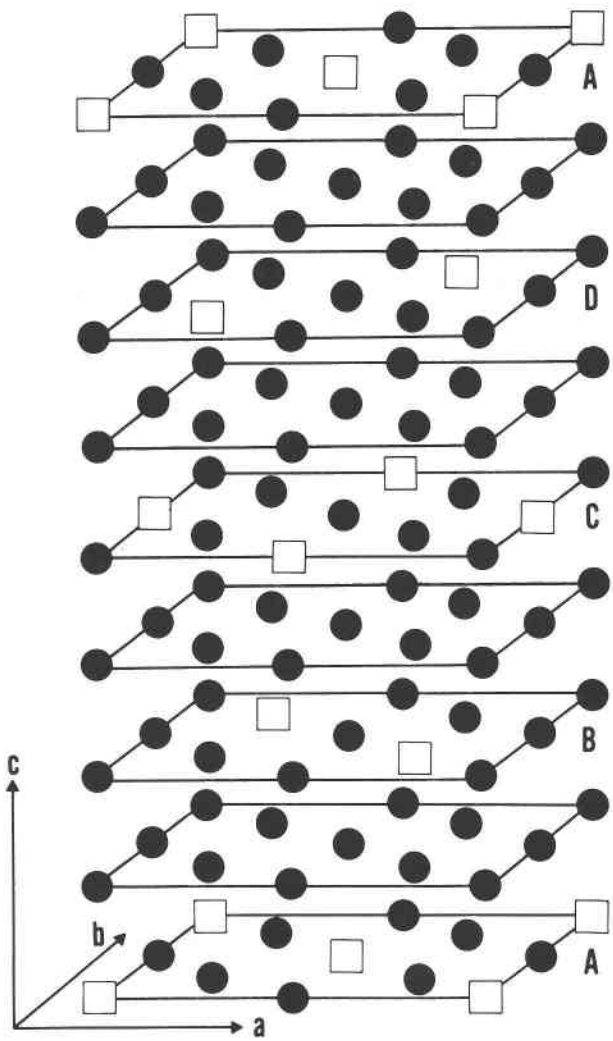

FIG. 1. The metal vacancies in the 4*C* type pyrrhotite (Bertaut, 1953) based on space group $F2/d$. Only Fe layers are indicated for simplicity. Squares representing vacant sites in different layers are named as A, B, C, and D.

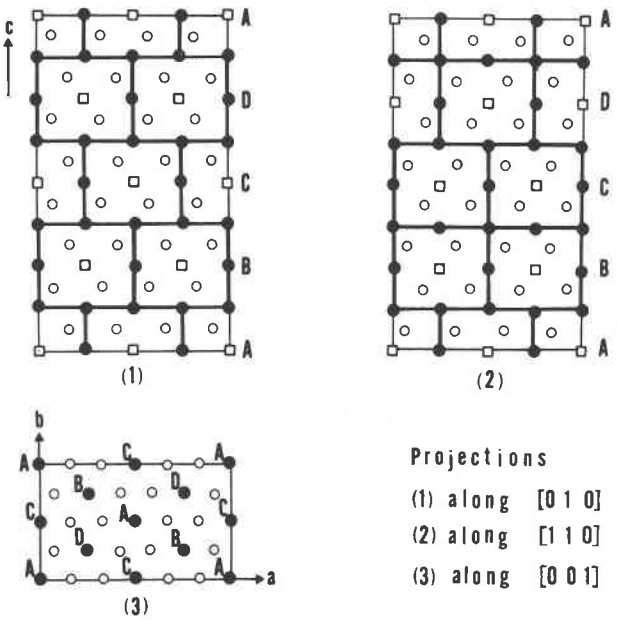

FIG. 2. Two-dimensional structures of the 4*C* type pyrrhotite projected along (1)[010], (2)[110], and (3)[001], of the 4*C* type cell. Iron sites with and without vacancy are indicated by large black circles and open squares respectively, and sulfur atom sites are indicated by small open circles.

D. F represents completely filled layers. If the filled layers are omitted for simplicity, the structure is represented as ABCDABCD· · · · ·.

The structure projected along [010], [110], and [001] is illustrated in Figure 2. Slight displacements of atoms from their ideal positions are neglected. Directions [010] and [110] of the 4*C* type correspond to [100] and [010] of the hexagonal NiAs cell. In the projections of Figure 2, two different Fe sites are shown: those entirely occupied by Fe atoms (large black circles) and those which are only half occupied by Fe atoms (open squares).

Results

A high magnification lattice image from the 4*C* pyrrhotite is reproduced in Figure 3. The true magnification 3×10^5 is calibrated using gold. The *c* axis is vertical to the image. The electron diffraction pattern included indicates the electron beam is parallel to [110] because $1\bar{1}1$ and $1\bar{1}3$ superstructure reflections are observed, with weak streaks connecting the two reflections. The main reflections correspond to the NiAs subcell. In this lattice image, the intervals between the nearest two white spots normal to the *c* axis (horizontal) and parallel to the *c* axis (vertical) are 5.9 and 5.7 Å, and correspond to $\sqrt{3}A$ and *C* respectively, where *A* and *C* are the dimensions of the fundamental NiAs cell. The unit cell of the 4*C* type is outlined in Figure 3. The dark rows and columns in Figure 3 correspond to the high atomic density regions representing S sites and non-vacant Fe sites. The white spots correspond to the low atomic density regions of vacant Fe sites.

Dark broad fringes occur parallel to the edge of the specimen in Figure 3, where the contrast and the details of the image are not clear. They are considered to be the thickness fringe due to main reflections such as $2\bar{2}0$ and $\bar{2}20$. Though these reflections are apparently eliminated by an objective aperture of 40 μm diameter in the diffraction pattern of Figure 3, their effect is observed in the micrograph. In order to confirm the contribution of the main reflections to the dark fringe, two different micrographs have been obtained from the same portion of the specimen (Fig. 4 A and B). For one (Fig. 4A) the incident beam was tilted so that the $\bar{2}20$ reflection was completely eliminated as observed in the diffraction pattern. No thickness fringe is observed in the micrograph. For the second image (Fig. 4B), however, a larger aperture of 60 μm diameter was used to include $2\bar{2}0$ and $\bar{2}20$ reflections. Formation of the dark fringe is clearly observed in the micrograph.

In Figure 3 two different kinds of bands are clearly observed normal to the *c* axis [or parallel to (001)]; they differ in the stacking sequence of the white spots, as can be best described by letting X represent a single layer of white spots in Figure 3 and by letting Y represent a similar layer whose white spots are displaced—by half the distance between the nearest white spots in a layer—relative to those of X. The one band, hereafter called XY, if projected along [010], is represented by the layer sequence XYXYXY . . . along the *c* axis and corresponds to the structure projected along [010] in Figure 2. The second kind of band, hereafter called XX, is represented by XXYYXXYY . . . . Single bands may contain from two up to ten stacked layers of white spots. The XY and XX bands are in a twin relation by three- or six-fold rotation about the *c** axis with the composition plane of (001). The twin boundaries are indicated on the right side of Figure 3. The diffuse streaks between $1\bar{1}1$ and $1\bar{1}3$ reflections in the electron diffraction pattern (Fig. 3) can be explained by the presence of successive stacking of narrow bands in twin relation and by the ratio of 1:2 for the area of XY bands and that of XX bands.

In the central part of Figure 3, a number of white streaks along the stacking layers are observed. The positions of the white spots gradually change through

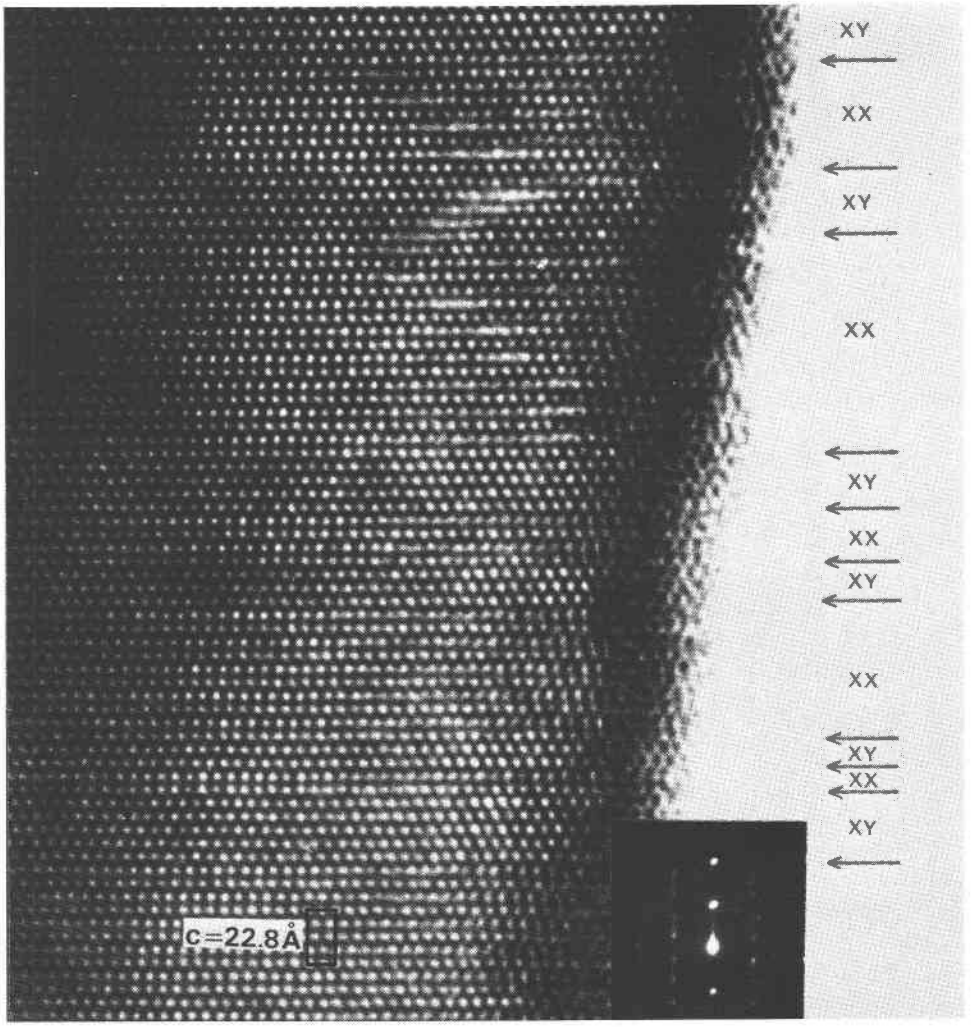

FIG. 3. High-resolution lattice image from the 4*C* type pyrrhotite at magnification of 4×10^6. The diffraction spots used for image formation are also indicated. The unit cell is outlined. The boundaries between XX and XY bands are indicated in the right side.

the streaks from X to Y, or *vice versa*, indicating existence of out-of-step boundaries across the streaks.

The band texture and the out-of-step boundaries are more clearly observed in the lattice image from the same portion of the specimen obtained at the range of underfocusing of about 200 ± 50 Å (Fig. 5A). The image contrast of this micrograph is a reversal of that obtained at 1100 ± 100 Å underfocusing (Figs. 3 and 5B).

Many structure images, obtained for different grains of the same specimen, have contrasts consistent with those explained above.

Discussion

In Figure 6A, an enlarged micrograph of Figure 3, the unit cells in the XY and XX bands are outlined. Two kinds of domain boundaries are clearly observed:

(a) twin boundaries parallel to (001),
(b) out-of-step boundaries approximately parallel to $(10\bar{2})$ in the XY band and to its symmetrically related plane $(\bar{1}14)$ in the XX band.

A part of Figure 6A is schematically illustrated in Figure 6B where the twin and out-of-step boundaries are indicated with the same magnification as in Figure 6A. The details of these boundaries and their genesis are discussed below.

(a) Twin Boundaries

According to the precession method, the crystals used in this investigation are monoclinic and have a β

angle of 90.47°. The XX bands and XY bands are parallel and in contact along (001). The deviation of the β angle from 90° takes place by a very slight displacement from the ideal position of each stacking layer along [100]. The displacement of the stacking layers is greatest in the XY bands, because it is the projection on (010). The effect of the displacement is, however, observed neither in the XY bands nor in the XX bands (Figs. 3, 6A), possibly because the thickness of the bands is not enough to make the small deviation of β angles from 90° appreciable.

Therefore, the S layers and the filled Fe layers (dark region in Fig. 6A) are practically continuous through the twin boundary, and the twin relation in the 4*C* type takes place simply by the change of the arrangements of iron vacancies.

Because superstructure reflections indicating the twin relation are observed in the X-ray patterns, the fine twin texture is not considered to be a characteristic feature of the thin fragments and thus mechanically induced in preparation, but is considered to exist in the original specimen.

(b) Out-of-Step Boundaries

The streaks due to the out-of-step boundaries appear in each layer in the XY bands, but only in alternate layers in the XX bands (Fig. 6A).

As previously explained, the 4*C* structure type is represented as stackings of ABCD - - - , if we omit the filled Fe layers and S layers for simplicity. To present vacancies at A sites occupying X positions in the lattice image, a notation A(X) is used. Then the XY

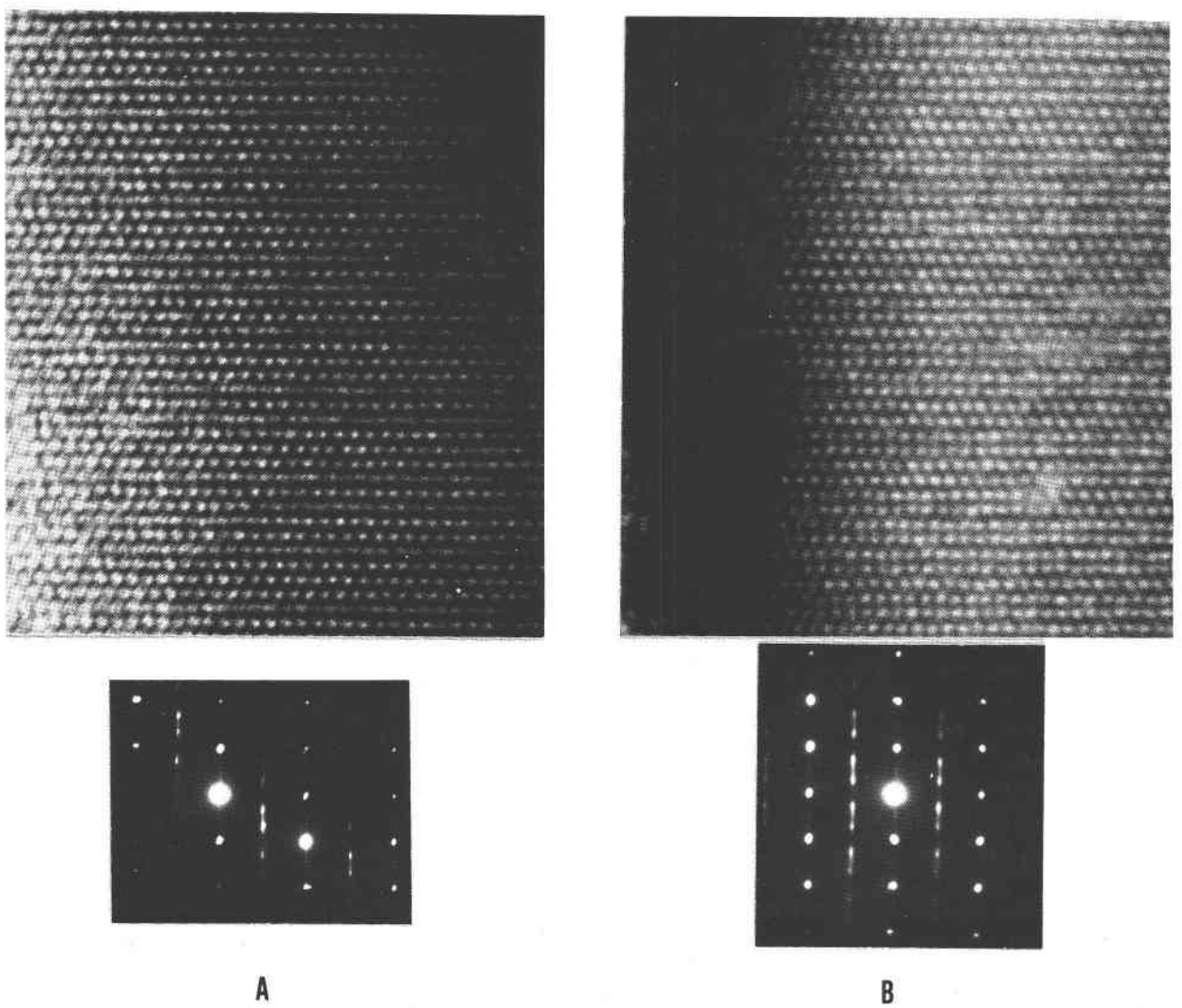

FIG. 4. Two lattice images from the same position of the 4*C* type specimen at two different diffraction conditions: tilting incident beam with a small aperture (A) and no tilting of the incident beam with a large aperture (B). The diffraction patterns are also reproduced.

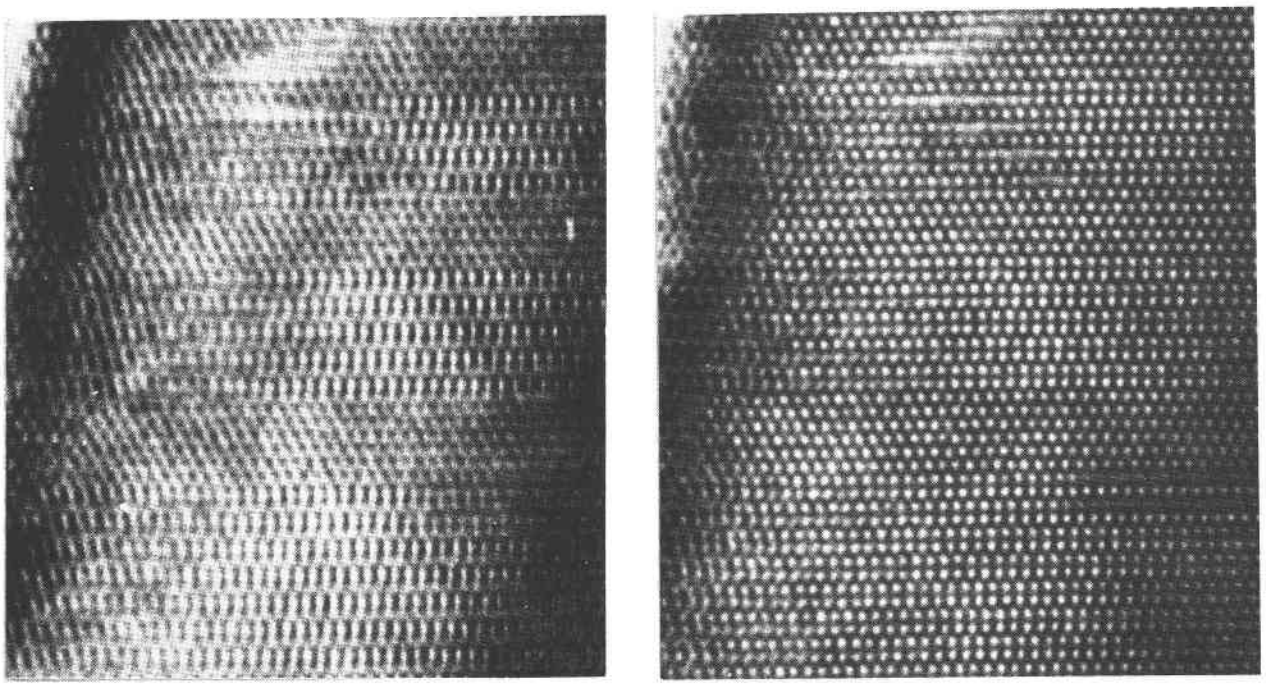

FIG. 5. Lattice image from 4*c* type pyrrhotite obtained at about 200 ± 50 Å underfocus (A), compared with that taken at 1100 ± 100 Å underfocus (B). Narrow band textures due to successive twin boundaries normal to the *c* direction and out-of-step boundaries are clearly observed, but the image contrast of Figure 4A is the reverse of that of Figures 3 and 4B.

bands are represented as A(X)B(Y)C(X)D(Y) - - - and the XX bands as A(X)B(Y)C(Y)D(X) – – –.

If we consider an out-of-step displacement by a vector of **c**/4, the following changes of the vacancy sites in the XY and XX bands are given:

(a) XY band	(b) XX band
D(Y) ⟶ A(X)	D(X) ⟶ A(X)
C(X) ⟶ D(Y)	C(Y) ⟶ D(X)
B(Y) ⟶ C(X)	B(Y) ⟶ C(Y)
A(X) ⟶ B(Y)	A(X) ⟶ B(Y)

In each band, the original stacking of the defective layers at the left side changes to a new stacking at the right side through the out-of-step boundaries. The streaks at the out-of-step boundaries in the lattice image take place by the scattered distribution of the vacant sites to the consecutive X and Y sites, which is caused by the superposition of the left and right domains at the inclined boundaries. In Figure 6B, the usual white spots are represented by large circles and the streaks by a series of small circles occupying the consecutive X and Y sites.

Because the length of the streaks is very short compared with the thickness of the specimen along the electron beam, the boundaries must be almost perpendicular to the projection plane and parallel to $(10\bar{2})$ in the XY bands and to its symmetrically related plane $(\bar{1}14)$ in the XX bands (Fig. 6B). These planes are the densest ones next to (001) in structures of the 4*C* type. It is reasonable to assume that the twin and out-of-step boundaries take place along the densest planes in the structure. Although the out-of-step boundaries disappear at the twin boundaries, it is not clear whether the apparent displacement of **c**/4 between domains has really taken place.

(c) Genesis of the Domain Textures in the 4C Type

The successive stacking of narrow bands in a twin relation can be understood by assuming that the specimen originally crystallized as the 1*C* or NiAs type with disordered arrangement of vacancies above 300°C, and then rapidly transformed to the 4*C* type. Because the 1*C* type is hexagonal, the twin bands were introduced in the transition to the monoclinic 4*C* type to reduce the strain caused by the transition minimum. The out-of-step boundaries are considered to be introduced in transition or after transition.

Success in interpretation of the lattice image of the 4*C* type pyrrhotite based on its known structure has

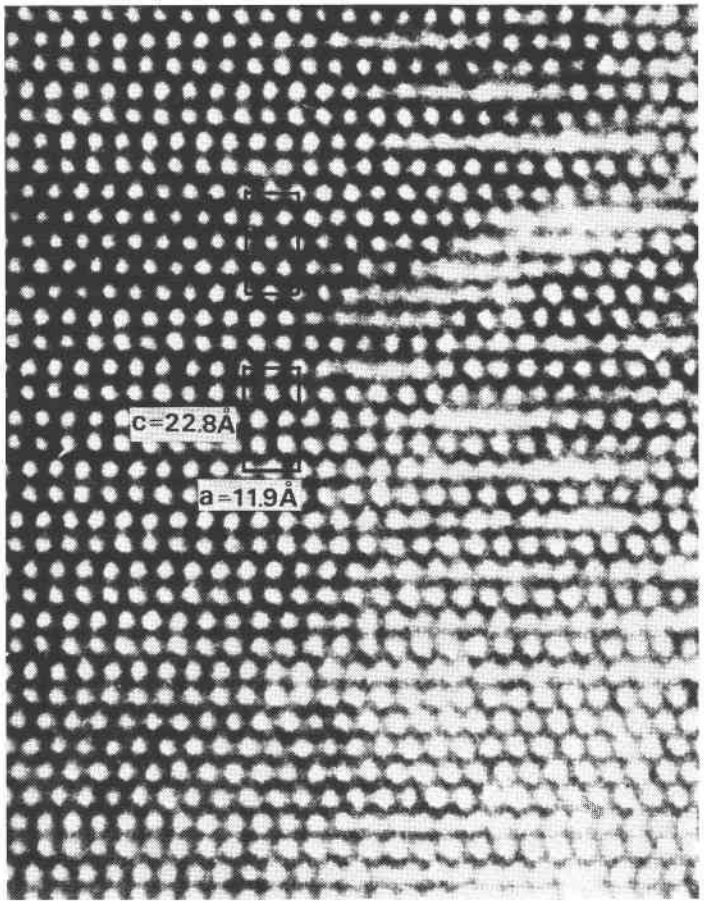

A

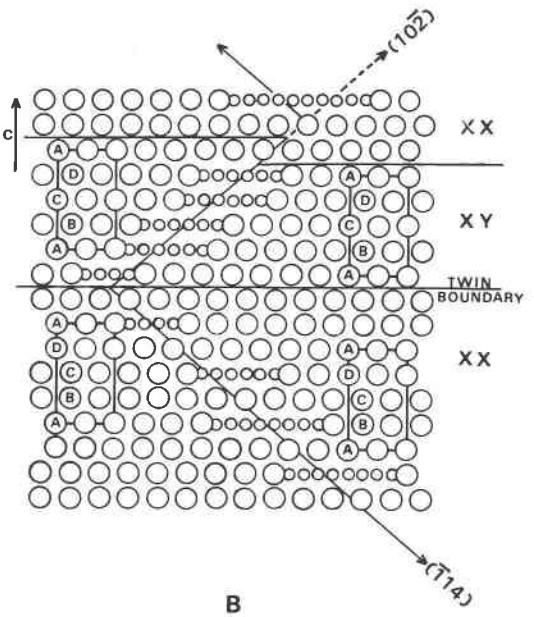

B

FIG. 6. A. High magnification lattice image from the 4*C* type pyrrhotite showing the twin and out-of-step boundaries. The unit cells in the XY band (upper) and XX band (lower) are outlined. B. Schematic representation of the twin and out-of-step boundaries in the structure of 4*C* type pyrrhotite corresponding to Figure 6A. The usual white spots are represented by large circles and the streaks by a series of small circles occupying the consecutive X and Y sites.

established that the high-resolution electron microscope is a powerful technique for studying the superstructures of pyrrhotites. The study of non-stoichiometric pyrrhotite has also been carried out based on the results of the 4*C* type pyrrhotite (Nakazawa, Morimoto, and Watanabe, 1974b).

Acknowledgments

The authors express their thanks to Drs. M. Tokonami, K. Koto, and T. Osaka for their valuable comments and discussions. Dr. S. Banno and Mr. T. Itaya kindly made the EPMA analysis of the pyrrhotite specimen. The authors also thank Miss M. Hirano and Miss H. Iijima for typing the manuscript.

Part of the cost of this study was defrayed by a research grant from the Ministry of Education of Japan.

References

ALLPRESS, J. G., AND J. V. SANDERS (1973) The direct observation of the structures of real crystals by lattice imaging. *J. Appl. Crystallogr.* **6**, 165–190.

ARNOLD, R. G. (1962) Equilibrium relation between pyrrhotite and pyrite from 325° to 743°C. *Econ. Geol.* **57**, 72–90.

BERTAUT, E. F. (1953) Contribution a l'etude des structures lacunaires: la pyrrhotine. *Acta Crystallogr.* **6**, 557–561.

BUSECK, P. R. AND S. IIJIMA (1973) High resolution electron microscopy of silcates. *Amer. Mineral.* **59**, 1–21.

IIJIMA, S., AND J. G. ALLPRESS (1973) High resolution electron microscopy of $TiO_2 \cdot 7Nb_2O_5$. *J. Solid State Chem.* **7**, 94–105

———, AND ——— (1974) Structural studies by high-resolution electron microscopy: tetragonal tungsten bronze-type structures in the system Nb_2O_5–WO_3. *Acta Crystallogr.* **A30**, 22–29.

MORIMOTO, N., A. GYOBU, H. MUKAIYAMA, AND E. IZAWA (1975a) Crystallography and stability of pyrrhotites. *Econ. Geol.* (in press).

———, ———, K. TSUKUMA, AND K. KOTO (1975b) Superstructure and nonstoichiometry of the intermediate pyrrhotite. *Am. Mineral.* **60**, 240–248.

———, H. NAKAZAWA, AND E. WATANABE (1974) Direct ob-

servation of metal vacancy in pyrrhotite, $Fe_{1-x}S$, by means of electron microscopy. *Proc. Japan Acad.* **50,** 756–759.

NAKAZAWA, H., AND N. MORIMOTO (1971) Phase relations and superstructures of pyrrhotite, $Fe_{1-x}S$. *Mat. Res. Bull.* **6,** 345–358.

———, ———, AND E. WATANABE (1974a) Direct observation of pyrrhotite (Fe_7S_8) by electron microscopy. *Abstr. Int. Crystallogr. Conf. Diffraction Studies on Real Atoms and Real Crystals,* p. 223–224.

———, ———, AND ——— (1974b) Direct observation of the non-stoichiometric pyrrhotite. *Proc. 8th Int. Congr. Electron Microscopy,* **1,** 498–499.

TOKONAMI, M., K. NISHIGUCHI, AND N. MORIMOTO (1972) Crystal structure of a monoclinic pyrrhotite (Fe_7S_8). *Am. Mineral.* **57,** 1066–1080.

VAN LANDUYT, J., AND S. AMELINCKX (1972) Electron microscope observations of the defect structure of pyrrhotite. *Mat. Res. Bull.* **7,** 71–80.

Manuscript received, November 5, 1974; accepted for publication, February 5, 1975.